Model-building with image segmentation and fast image updates

Adam Halpert and Gboyega Ayeni

ABSTRACT

An accurate salt interpretation is an essential component of velocity model-building in areas dominated by complicated salt geology. The Pairwise Region Comparison (PRC) image segmentation algorithm can automatically pick salt bodies on seismic images, and be used as part of an iterative sediment-flood and salt-flood model-building workflow. In areas where the salt interpretation is highly uncertain, however, human expertise is needed to judge the relative accuracy of two or more possible models. We demonstrate a fast image updating scheme based on shot-profile migration that can be used to investigate how different salt interpretations provided by the PRC algorithm affect the final image. With further efficiency improvements, this process could allow for an interactive interpretation, model-building, and imaging workflow that substantially reduces cycle time for large-scale iterative imaging projects.

BACKGROUND

The goal of any automated seismic image segmentation scheme is to automatically pick out or delineate regions within a seismic image. Salt interpretation is an especially useful application of this technology; large, subsurface salt bodies can be tedious and very time-consuming to interpret manually, but the sharp salt/sediment velocity contrast makes an accurate interpretation essential for building a satisfactory velocity model. This means that we should not rely solely on an automatic salt interpretation, but should instead draw on the expertise of experienced human interpreters to supplement the process. This can be accomplished in a variety of ways; for example, a manual 2D interpretation can be used to guide an automatic 3D segmentation (Halpert, 2011). A complementary option is to use human expertise to choose the best of several possible interpretations provided by an automatic algorithm. Here, we demonstrate one such strategy using fast image updates to examine differences between possible models.

The "Pairwise Region Comparison" (PRC) seismic image segmentation approach (Halpert et al., 2010; Halpert, 2010) relies on the graph-based segmentation method of Felzenszwalb and Huttenlocher (2004). This method is more efficient than eigenvector-based algorithms such as Normalized Cuts Image Segmentation (Shi and Malik, 2000; Lomask, 2007), and is capable of operating on full seismic images. Here, the PRC

method is used on images from the Sigsbee 2A synthetic model to provide two possible top-salt interpretations. Then, a fast image-update scheme based on shot-profile migration is used to examine how an image changes as a result of the two interpretations.

SEGMENTATION PROCESS

Under ideal cirmucmstances, automated segmentation using the PRC method can provide a quick and accurate interpretation of regions within a seismic image. For example, the image in Figure 1(a) is a perfect-velocity migration of data from the Sigsbee synthetic model. In the corresponding segmentation result (Figure 1(b)), the salt body is delineated clearly and accurately. Unfortunately, perfect velocity models are non-existent in the real world. Instead, a common approach to building a velocity model in areas dominated by complex salt geology is to pick the top salt after migration with a sediment-flood velocity model, and then pick the base of salt after migration with the resulting salt-flood velocity model (Mosher et al., 2007). It is clear from Figure 2(a), a sediment-flood migration zoomed in to the left half of the salt body, that the salt boundary of a sediment-flood image is not likely to be imaged as well as the perfect-velocity example in Figure 1(a). The resulting segmentation of the image into above- and below-salt regions (Figure 2(b)) is therefore not as accurate.

Since the major source of inaccuracy in the Figure 2(b) result is within the salt canyon indicated on the figure, we can restrict our analysis to that region. By setting a smaller minimum segment size, the user can be much more selective about what regions to include as salt. Figures 3(a) and 3(b) display two possible salt interpretations generated by the automatic PRC algorithm for the region in question. In Figure 3(b), an extra segment (indicated by the arrow) has been included in the salt. By replacing segments interpreted as salt with salt velocities on the original sediment flood velocity model, two different velocity models can also be created (Figures 4(a) and 4(b)).

IMAGE UPDATES

Image updates and comparisons will be performed using *shot-profile migration* (see Biondi (2005)). In general, this type of migration uses downward-continued source (P^s) and receiver (P^g) wavefields:

$$P^s_z = P^s_{z=0} e^{-ik_z z} \tag{1}$$

$$P^g_z = P^g_{z=0} e^{ik_z z}, \tag{2}$$

where z is the depth and k_z is the vertical wavenumber calculated in a split-step fashion (Stoffa et al., 1990) for a given frequency ω according to

$$k_z = \sqrt{\frac{\omega^2}{v^2_{\text{ref}}} - |\mathbf{k}|^2} + \left(\frac{\omega}{v(z,x)} - \frac{\omega}{v_{\text{ref}}} \right), \tag{3}$$

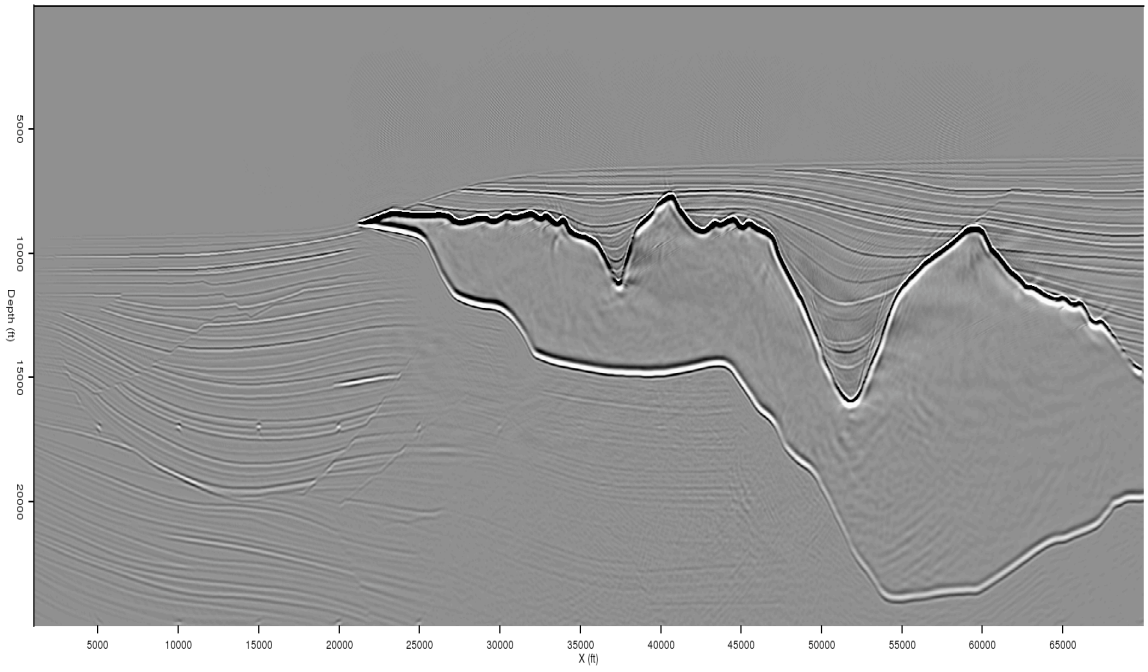

(a)

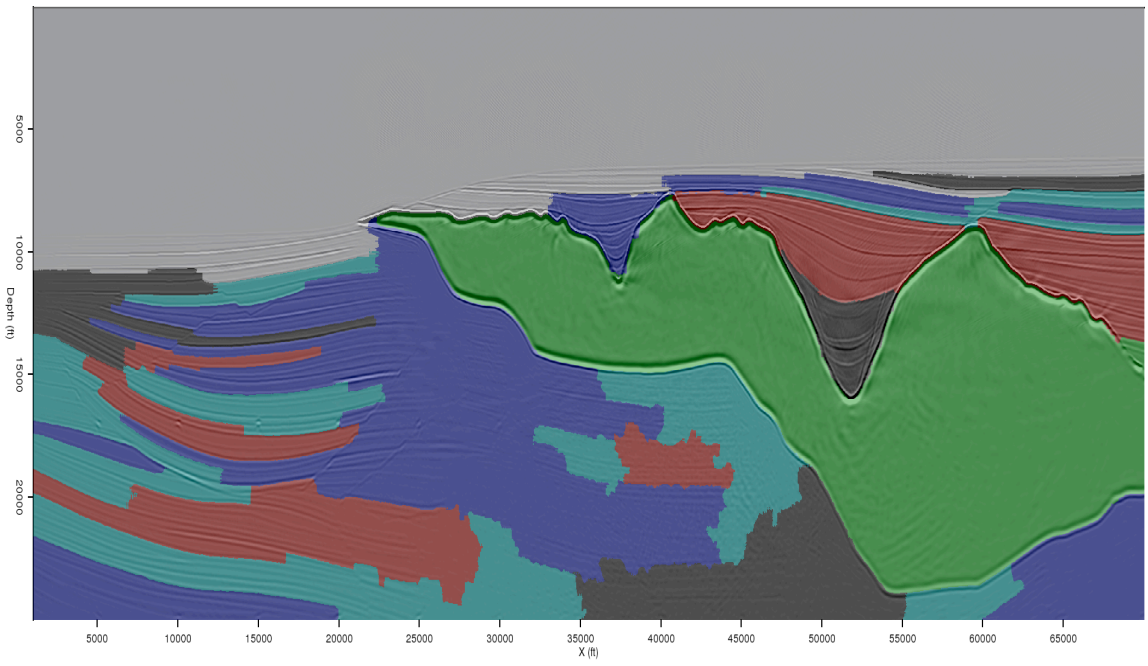

(b)

Figure 1: Perfect-velocity image (a) and automatic segmentation result (b) from the Sigsbee synthetic model. In (b), the salt body has been interpreted nearly perfectly. [**ER**]

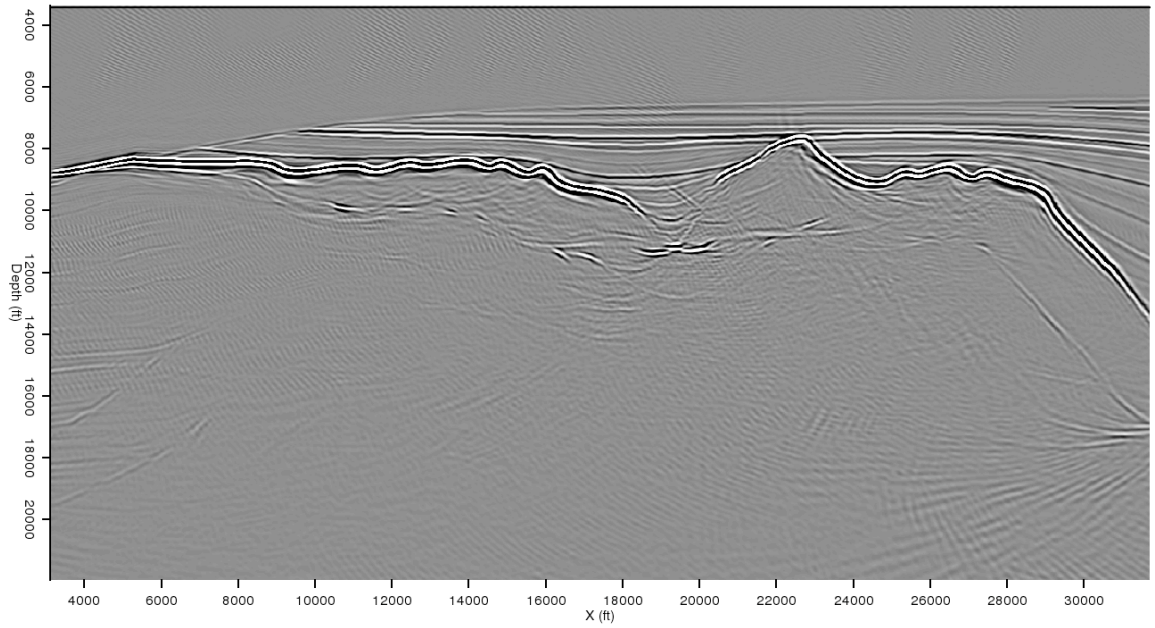

(a)

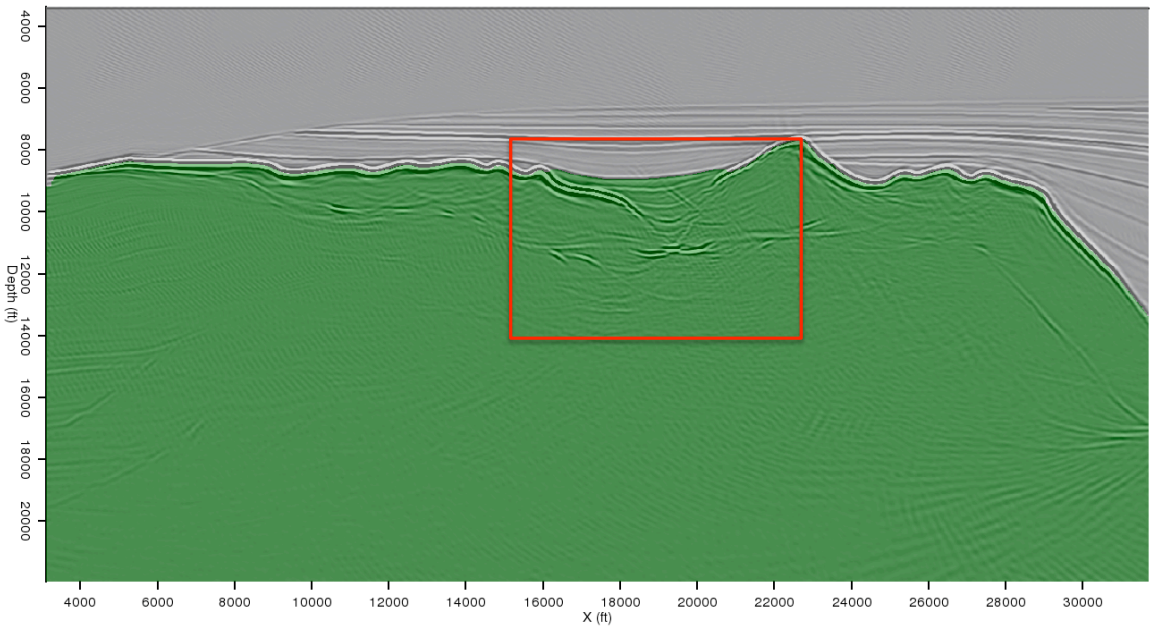

(b)

Figure 2: Sediment-flood migration (a), and corresponding segmentation result (b). The segmentation algorithm performs poorly within the area indicated on (b). [**CR**]

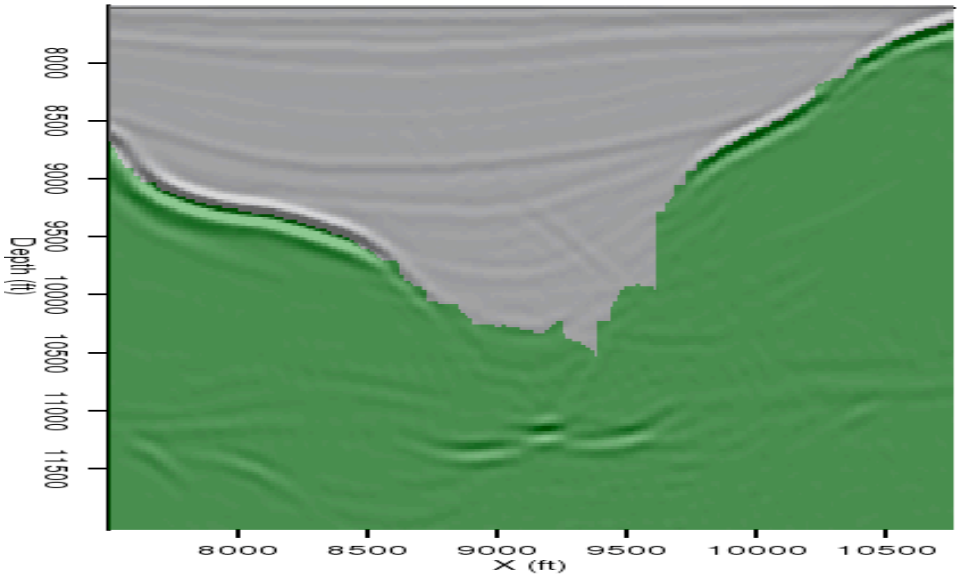

(a)

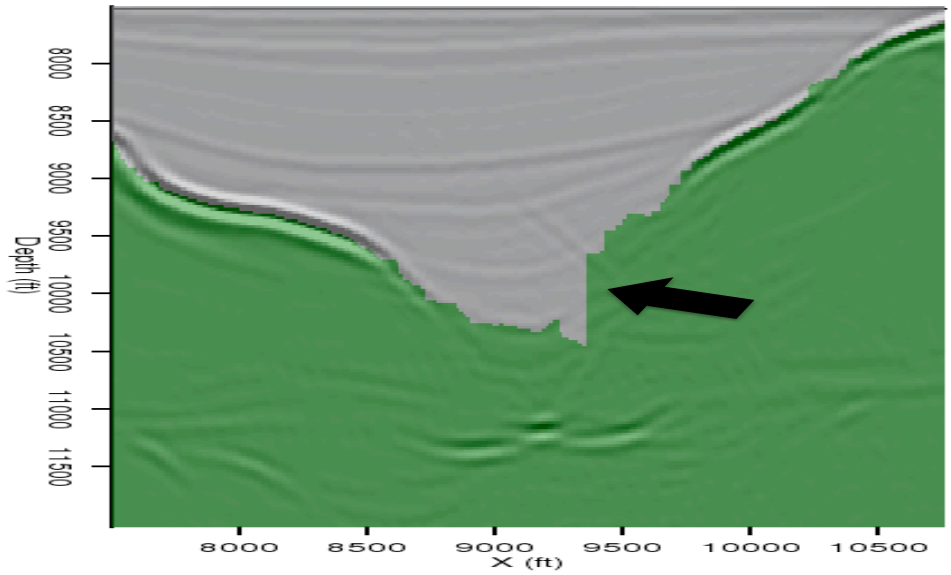

(b)

Figure 3: Two possible salt interpretations provided by the segmentation algorithm. In (b), an extra segment (indicated by the arrow) has been included in the salt. [**CR**]

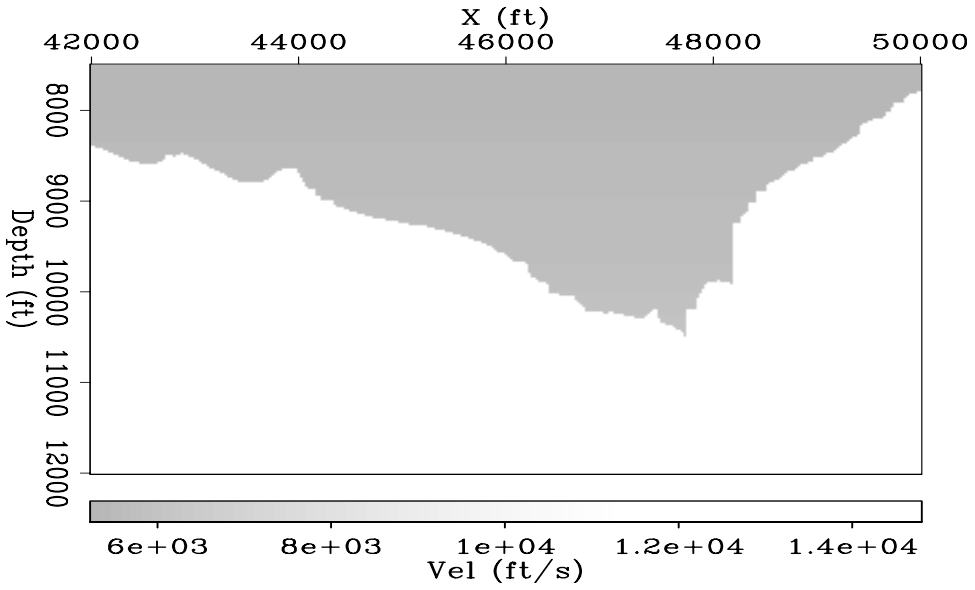

(a)

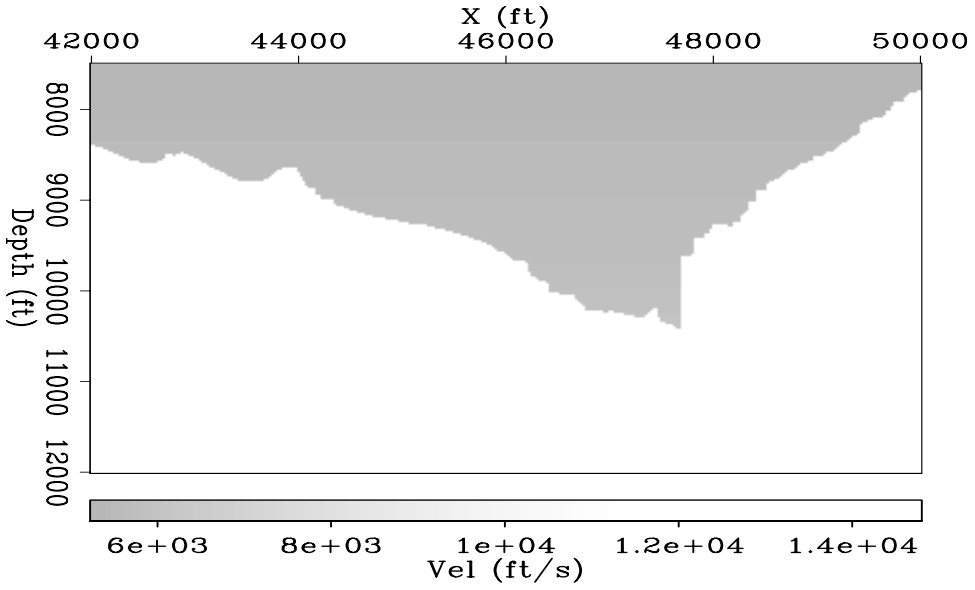

(b)

Figure 4: Salt-flood velocity models corresponding to the interpretations in Figures 3(a) and 3(b). The models were created from a sediment-flood velocity model by assigning salt velocities below the interpreted salt boundary. [**CR**]

where $\mathbf{k}$ is a vector containing the horizontal wavenumbers. Here, v_{ref} is a reference velocity that is constant at each depth step, while $v(z,x)$ is the actual estimated velocity. An image is formed by correlating the two wavefields:

$$I(z,x) = \sum_i \sum_\omega P_z^g(\omega, x; \mathbf{s}_i)\overline{P_z^s(\omega, x; \mathbf{s}_i)}. \tag{4}$$

Performing full migrations is impractical for our stated purpose of allowing interpreters to quickly judge the relative accuracy of two or more possible velocity models. One way to speed up the process is to re-datum the wavefields to a depth just above the region of interest – in this case, just above the salt canyon near $z = 7500$. If we only wish to investigate changes in a specific area of the image, we can downward continue both wavefields to this level, and inject areal source and receiver gathers. This allows us to obtain comparison images like those in Figure 5(a) and 5(b), at a computational cost an order of magnitude less than performing full migrations like the one in Figure 1(a). In this case, it is clear that the salt canyon flanks in Figure 5(a) are more sharply focused, so the salt interpretation and velocity model in Figures 3(a) and 4(a), respectively, are more accurate.

GENERALIZED WAVEFIELDS AND PHASE ENCODING

While restricting the domain and datuming the wavefields as described above significantly lessened the computational expense of updating the image, the process still occurs over a matter of minutes, rather than the seconds required to approach the level of interactivity we seek. One possibility to improve the performance of shot-profile migration is to use *phase encoding* (Romero et al., 2000), in which data from N shots are combined into a generalized source gather:

$$\hat{P}(\omega, x; j) = \sum_{i=1}^{N} \epsilon_{i,j}(\omega) P(\omega, x; \mathbf{s}_i). \tag{5}$$

Here, the ϵ term is a complex weight value assigned to each shot.

A simple experiment combines all shots into a single generalized source gather, and uses a single generalized plane-wave source function for migration. Figure 6 is the perfect-velocity image resulting from this procedure. While information from unwanted crosstalk terms have significantly degraded the image, the salt body and its boundaries are still visible. When the two possible salt-flood velocity models in Figures 4(a) and 4(b) are used, we obtain the zoomed-in images in Figures 7(a) and 7(b), respectively. While the differences between these two images is not as apparent as for Figures 5(a) and 5(b), the salt canyon walls appear more continuous for the first model, especially near the location indicated by the arrow. These migrations were completed in less than five seconds; although this is only a 2D example, this is approaching a level at which interactive imaging becomes feasible.

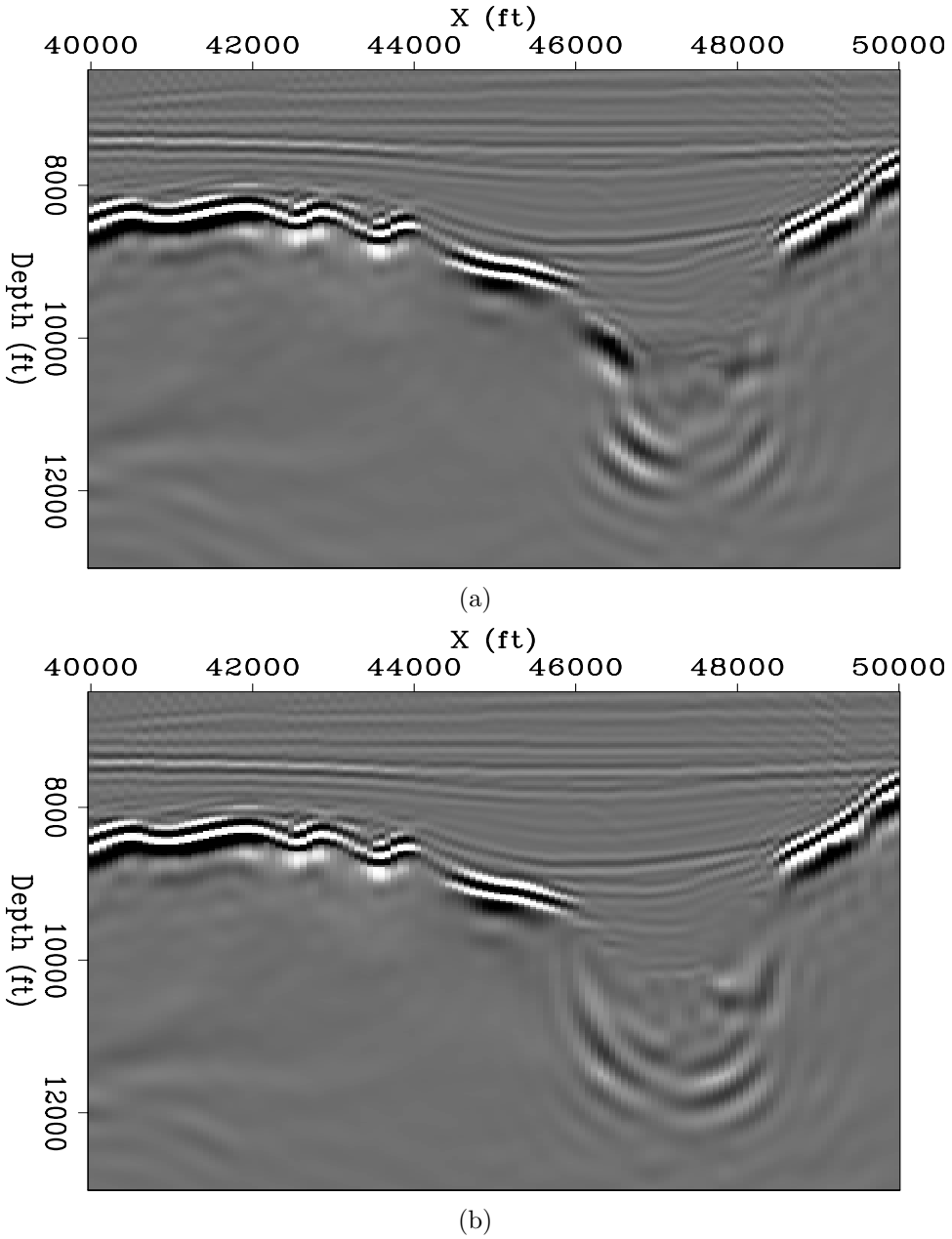

Figure 5: Images resulting from the velocity models in Figures 4(a) and 4(b). The salt canyon walls are more focused in (a), indicating the the salt interpretation in Figure 3(a) is more accurate. [**CR**]

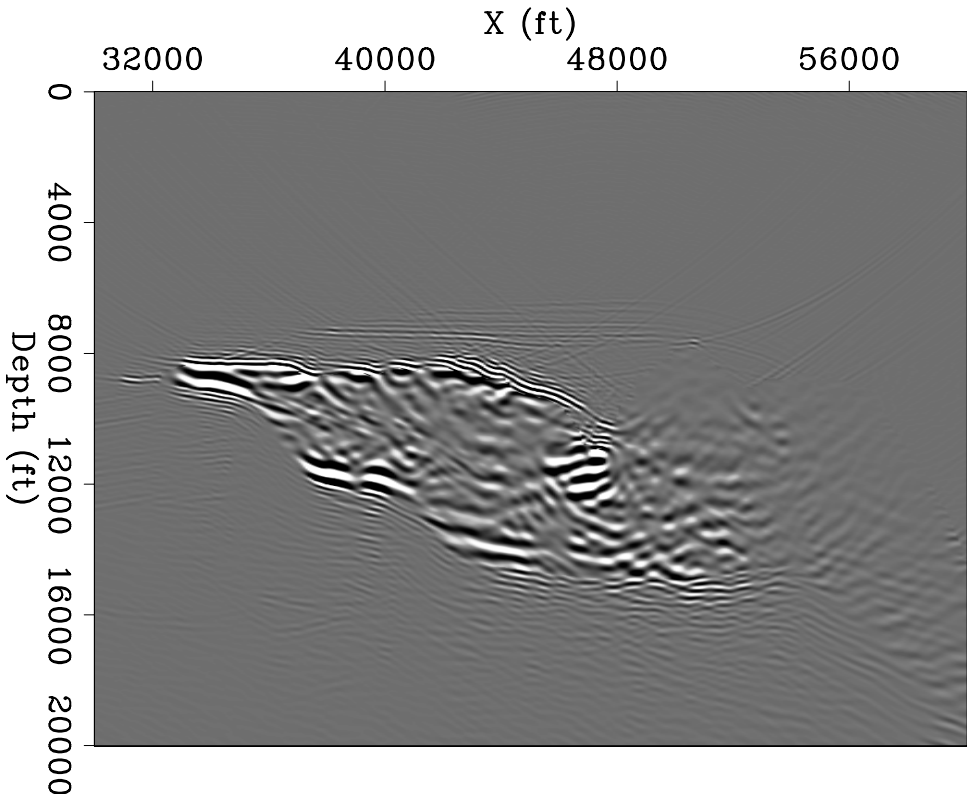

Figure 6: A perfect-velocity migration in which all shots have been combined into a single generalized source gather, and a single plane-wave is used as the generalized source function. Crosstalk artifacts have significantly degraded the image, but the salt body is still clearly visible. [**CR**]

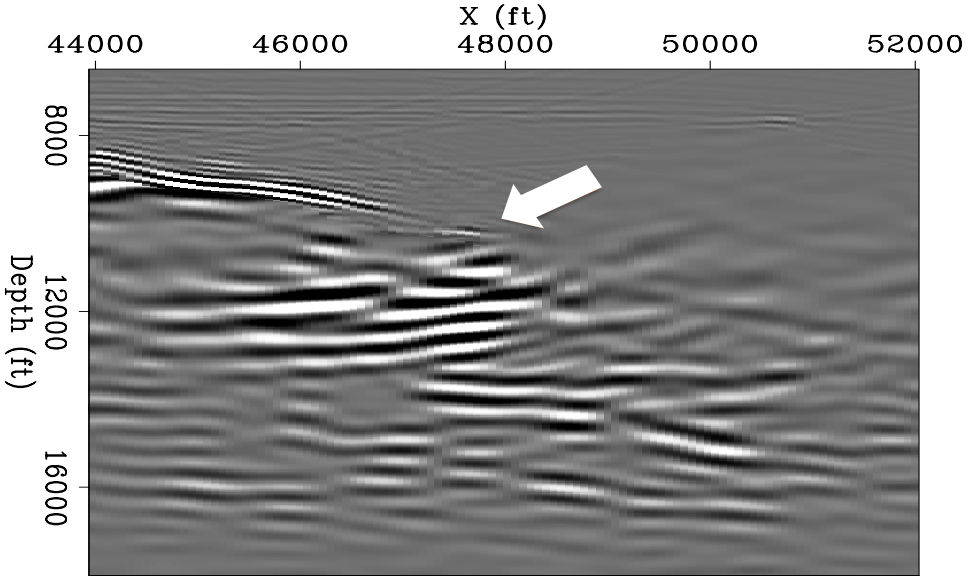

(a)

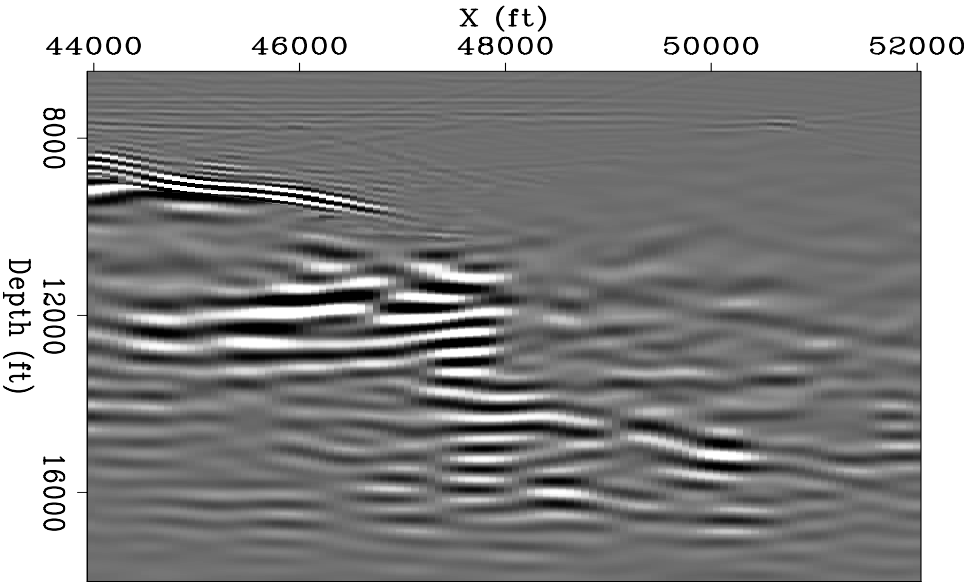

(b)

Figure 7: Generalized wavefield migrations corresponding to the velocity models in Figures 5(a) and 5(b). While crosstalk artifacts obscure the differences between the two images to a much greater extent than in Figures 5(a) and 5(b), the salt canyon wall is still noticeably more continuous near the indicated location in (a). [**CR**]

Further improvents are necessary to obtain cleaner images than in Figures 6, 7(a) and 7(b). One option is to define the weighting coefficients from equation 5 as having only imaginary (phase) components:

$$\epsilon_{i,j}(\omega) = \frac{e^{i\phi_{i,j}}(\omega)}{\sqrt{M}}, \tag{6}$$

where M is the number of generalized sources. By making ϕ a random phase function, it is possible to attenuate the crosstalk terms that arise from combining information from different shots (Morton and Ober, 1998). The implementation of a scheme combining image segmentation, re-datumed wavefields and phase-encoding could allow interpreters to interactively view high-quality images of several salt-interpretation scenarios.

CONCLUSIONS

The Pairwise Region Comparison (PRC) image segmentation algorithm can function effectively as part of an iterative salt interpretation and model-building workflow. However, segmentation results have a higher degree of uncertainty when a boundary is faint or discontinuous (for example, on a sediment-flood image). In such cases, a targeted shot-profile migration scheme using datumed wavefields can test two or more possible models relatively quickly, allowing an interpreter to judge each model's accuracy either qualitatively or quantitatively (e.g., flatness of angle gathers). The use of generalized wavefields further reduces the computational expense of testing multiple salt-interpretation scenarios. With additional improvements, such as the inclusion of phase-encoding migration to improve the quality of images, this scheme could form the basis of an interactive interpretation and model-building workflow.

ACKNOWLEDGMENTS

We thank SMAART JV for providing the Sigsbee 2A model used for examples, and the sponsors of the Stanford Exploration Project for their support.

REFERENCES

Biondi, B., 2005, 3-D seismic imaging: Stanford University.

Felzenszwalb, P. F. and D. P. Huttenlocher, 2004, Efficient graph-based image segmentation: International Journal of Computer Vision, **59**, 167–181.

Halpert, A., 2010, A new method for more efficient seismic image segmentation: SEP-Report, **140**, 213–228.

———, 2011, Interpreter input for seismic image segmentation: SEP-Report, **143**, 237–248.

Halpert, A., R. G. Clapp, and B. L. Biondi, 2010, Speeding up seismic image segmentation: SEG Technical Program Expanded Abstracts, **29**, 1276–1280.

Lomask, J., 2007, Seismic volumetric flattening and segmentation: PhD thesis, Stanford University.

Morton, S. A. and C. C. Ober, 1998, Fastershot-record depth migrations using phase encoding: SEG Technical Program Expanded Abstracts, **17**, 1131–1134.

Mosher, C., E. Keskula, J. Malloy, R. Keys, H. Zhang, and S. Jin, 2007, Iterative imaging for subsalt interpretation and model building: The Leading Edge, **26**, 1424–1428.

Romero, L. A., D. C. Ghiglia, C. C. Ober, and S. A. Morton, 2000, Phase encoding of shot records in prestack migration: Geophysics, **65**, 426–436.

Shi, J. and J. Malik, 2000, Normalized cuts and image segmentation: Institute of Electrical and Electronics Engineers Transactions on Pattern Analysis and Machine Intelligence, **22**, 838–905.

Stoffa, P. L., J. Fokkema, R. M. de Luna Freire, and W. P. Kessinger, 1990, Split-step Fourier migration: Geophysics, **55**, 410–421.